Approaches to color and texture based image classification

Vidya Manian*, Ramón Vásquez

Department of Electrical and Computer Engineering
University of Puerto Rico, Mayagüez, PR 00681-9042

* Author to whom correspondence should be addressed. Ph: (787) 832 2825, Fax: (787) 832 2485,
E-mail: manian@ece.uprm.edu

ABSTRACT

A Gabor filtering method for texture based classification of color images is presented. The algorithm is robust and can be used with different color representations. It involves a filter selection process based on texture smoothness. Unichannel and interchannel correlation features are computed. Two types of color representations have been considered: (1) computing chromaticity values from xyY, HIS and RGB spaces and (2) using the 3 channels of the perceptually uniform color spaces L*a*b* and HSV. The RGB space universally used in image processing can be used for color-texture based classification by computing the *rgb* chromaticity values which yield higher classification accuracies than the direct use of R, G and B values. The wavelet transform methods have been extended to perform color image classifications with additional features. The two approaches: Gabor filtering and wavelet transform methods are compared in terms of classification accuracy and efficiency. The Pyramid Wavelet Transform (PWT) performs well with all color spaces. The Tree structured Wavelet Transform (TWT) is more suitable for smaller classification problems. The best color spaces for higher-class problems with wavelet methods are L*a*b* and HSV spaces. The HSV space is found to be the best for application of both the above texture based approaches. Computationally the Gabor method followed by PWT is fast and efficient.

Keywords: color, texture, color spaces, Gabor filters, wavelet transforms, image classification.

1. INTRODUCTION

Color is defined as that characteristic of a visible radiant power by which an observer may distinguish differences between *two structure-free fields* of view of the same size and shape, such as may be caused by differences in the spectral composition of the radiant power concerned in the observation [1]. While texture can be loosely defined as the structural pattern of surfaces such as wood, grain, grass *which is homogeneous in spite of fluctuations in brightness and color* [2]. A *color-texture* is a "*chromatic or colored structural pattern*" and a color-texture combined cue can be defined as "the visible radiant power and visual regular structural pattern using which an observer may distinguish between two objects". As the definition suggests, a system that combines the effect of color and texture will be more effective and is therefore more desirable.

In image classification several texture-based algorithms have been developed which include statistical feature extraction methods, structural, random field, spectral and neural network methods [3] for analysis, synthesis, classification and segmentation. Recently, multiresolution wavelet methods have gained a lot of attention [4,5,6,7]. Wavelet transform methods [7] have been used for image classification. Gabor filtering approaches have also been widely used for image segmentation [8]. All the above methods have been applied to gray scale images with pixel values from 0 to 255. Classification of color images has also been done by mapping the three channels R, G and B to gray scale values.

Color cues have been used for visual monitoring, surveillance [9], for image retrieval from databases [10,11,12] and for color device calibration [13]. Investigation in classification of color images has received some attention but not as much as gray level images. To name a few from the literature, color features have been used for texture recognition [14], using a Gabor based multiscale representation. Multispectral random field models have been developed to analyze color textures [15,16]. It has been found that the response of the human visual system depends on frequency of spatial distribution of colors [17]. When different color schemes are present it is important to analyze each space and obtain a best representation for good classification accuracy. In [18] the L*a*b* and HSV spaces have been found to outperform the RGB space using Gabor filters, with a maximum classification accuracy of about 82%. However, the performance of RGB space can be improved by computing chromaticity values as shown in this work. In [19] wavelet covariance signatures are used for classifying color images, but only linear transform spaces have been considered. A robust method that is adaptive to different color spaces is needed as the performance of a system should not be limited by the choice of the color space. In this paper a Gabor filtering approach adaptive to different color spaces is presented and also wavelet methods are implemented to yield efficient features for color-texture based image classification. Different color spaces are compared and analyzed. The advantage of using the above methods with color images in terms of performance and computational aspect is discussed. The paper is organized as follows. Section 2 describes the color spaces considered. Section 3 describes the Gabor filtering method and the wavelet methods used for the classification process. Section 4 presents experimental results and observations. Discussion and conclusions are presented in Section 5.

2. COLOR SPACES

Color measures are treated by the science of colorimetry which measures color qualitatively, and luminance measures are subject of the science of photometry [20]. Color is perceived as per its brightness, hue and saturation. Brightness is the perceived luminance. The hue refers to the amount of redness, greenness of the image. Saturation varies and is stronger as more and more white light is added to a monochromatic light. All of the three components change when either the wavelength, the intensity, the hue, or the amount of white light in a color is changed. Additive and subtractive color matching techniques are available. In colorimetry the measurements are in terms of the tristimulus values of a color. For image processing apart from knowing the relative amount of light from each primary the absolute value has to be determined which is the luminance. RGB image is based on primary relative color. This space does not represent color as perceived and analyzed by the human visual system. Studies are still in progress on how the brain receives the data from the L, M and S cones and other cells and processes the scenes. But, a basic factor known is that the human visual system uses three paths one for achromatic information and two for chromatic contrast signals [21]. Color information has been used in two ways. In the first case, the chrominance and luminance values computed from the xyY, HIS and RGB color spaces are used. In the second case, all the three color channels of the perceptually uniform color spaces L*a*b* and HSV are considered.

2.1 Chromaticity computation

Chromaticness or colorfulness is the attribute of a visual sensation according to which the perceived color of an area appears to be more or less chromatic [1]. This also quantizes the hue of the color. Hence, this information is sufficient to characterize color as defined by the tristimulus values. For the first case, the xyY and HIS transformations are applied to RGB images to extract chromaticity information. The transformation from RGB space to XYZ space and then to xyY are as follows [1]:

$$\begin{aligned} X &= 0.607R + 0.174G + 0.200B \\ Y &= 0.299R + 0.587G + 0.114B \\ Z &= 0.066G + 1.111B \end{aligned} \tag{1}$$

$$x = \frac{X}{X + Y + Z} \tag{2}$$

$$y = \frac{Y}{X + Y + Z} \tag{3}$$

In the xyY space, the Y values are the luminances and xy components have to be changed to a one dimensional chromaticity value (cr). The interval of the xy values (from 0 to 1) is divided in *p* intervals. This is a one-to-one mapping from a 2D space to 1D space as defined in [18]. The xy values are assigned to an equivalent value within 0 and *p*. *p* value used here is 5, which was chosen after some experimentation. Using the new equivalent value for each x and y the one dimensional chrominance value is given by the following formula:

$$cr = y + px \tag{4}$$

Fig 1 (a), (b) and (c) show the original food image and the chromaticity (cr) and luminance images (Y), respectively. The cr and Y values are used by the classification algorithms.

The chromaticity and luminance information can also be obtained from the HIS color space whose primaries are Hue (H), Intensity (I), Saturation (S). This space is described in [1]. The definition of H based on RGB space is

$$H = \arctan\left(\sqrt{3}(G - 2 * B)\big/(2 * R - G - B)\right) \tag{5}$$

$$I = \frac{R + G + B}{3} \tag{6}$$

The method adopted here follows from [1,18]. To quantize the H values to be assigned to pixels as [0 …255], first the arctan values are transformed from radians to degrees (i.e., from [0…2π] to [0°…360°]) using

$$H_1 = 180 * H + 180 \tag{7}$$

$$H_2 = \frac{H_1}{1.406} \tag{8}$$

These values are then mapped to [0…255] using Eqn. (8). The two channels H_2 and I that constitute the chromaticity and the luminance values are used. Fig. 1 (d) shows the H_2 image of Fig. 1 (a).

The chromaticity values for the RGB space are the chromaticity coordinates, which are the ratios of each tristimulus value of the color stimulus to their sum.

$$r(R,G,B) = \frac{R}{R + G + B},$$

$$g(R,G,B)=\frac{G}{R+G+B}, \tag{9}$$

$$b(R,G,B)=\frac{B}{R+G+B}$$

and $r+g+b=1$. The three channels r, g, b are used in the classification process.

2.2 Perceptually uniform color spaces

These spaces model closely the way in which the human visual system perceives color differences between two given color stimuli. They are considered here due to their similarity to the human visual system. The L*a*b* is a CIE (Commission Internationale de l'Eclairage) recommended approximately-uniform color space. The original space is the RGB which is converted to an intermediate CIE XYZ space and then to the L*a*b* space as below [1].

$$\begin{aligned} X &= 0.412453R + 0.357580G + 0.180423B \\ Y &= 0.212671R + 0.715160G + 0.072169B \\ Z &= 0.019334R + 0.119193G + 0.950227B \end{aligned} \tag{10}$$

$$\begin{aligned} L^* &= 116\, f\left(\frac{Y}{Y_n}\right) - 16 \\ a^* &= 500\left[f\left(\frac{X}{X_n}\right) - f\left(\frac{Y}{Y_n}\right)\right] \\ b^* &= 200\left[f\left(\frac{Y}{Y_n}\right) - f\left(\frac{Z}{Z_n}\right)\right] \end{aligned} \tag{11}$$

where

$$f(q)=\begin{cases} q^{1/3}, & \text{if } q > 0.008856 \\ 7.787q + 16/116, & \text{otherwise} \end{cases} \tag{12}$$

and $q \in \left\{ \frac{X}{X_n}, \frac{Y}{Y_n}, \frac{Z}{Z_n} \right\}$. The tristimulus values X_n, Y_n, Z_n are those of the nominally white object-color stimulus given by a CIE standard illuminant. For the illuminant D65 these values are obtained by setting R = G = B = 100 in (10). Here, L* is the luminance component. There are three channels in this space.

The HSV is also an approximately-uniform color space and is computed from the RGB space using procedure in [22]. The RGB values of the color image is mapped to HSV where the elements of H, S, and V are in the interval 0 to 1. The three output matrices constitute the Hue (H), Saturation (S) and color Values (V). The hue is equivalent to the chromaticity values, V to the luminance and S is the additional channel in this space.

3. ALGORITHMS FOR COLOR IMAGE CLASSIFICATION

3.1 Feature extraction using Gabor filtering method

In this method the images are filtered by Gabor filters [14] at different scales and orientations. The bank of filters in spatial domain is given by

$$f_{a,b}(x,y) = \frac{1}{2p\,s_a^2}\exp\left\{-\frac{x^2+y^2}{2s_a^2}\right\}\cos\left(2p\left(w_a x\cos q_b + w_a y\sin q_b\right)\right) \quad (13)$$

where a is the index for scale and b index for orientation. σ^2 is the variance. If $I_d(x,y)$ is the d^{th} channel of the color representation, the filtered image is

$$G_{dab}(x,y) = I_d(x,y) * f_{ab}(x,y) \quad (14)$$

3.1.1 Gabor Filter selection

For texture classifications it is not known which filter is best suitable for particular types of textures. The image samples are convolved with filters of orientations (0°,45°, 90°), frequencies (0.25, 0.50 and 0.75) and scales (σ = 0 to 1). The size of the filter has to be appropriately selected, depending on sample size and response characteristic. A procedure based on similarity of texture regions is applied, and a neighborhood energy measure is calculated to decide the best set of filters for textures that are coarse, fine and with dominant orientations. Using a neighborhood of 8 pixels in the response images $G_{dab}(x,y)$, the center pixel is replaced by a value obtained from:

$$Q_{rt} = \frac{\min(P_r, P_t)}{\max(P_r, P_t)} \quad (15)$$

where P_r is the center pixel and P_t is a neighborhood pixel. This measure is applied to each pixel by moving the window pixel by pixel. The Q_{rt} values are averaged for a window as below.

$$W_r = \frac{1}{8}\sum_{k=1}^{8} Q_{rt}^{k} \tag{16}$$

where k is the index of the eight neighboring pixels of the center pixel in the 3 x 3 pixel window. W_r is the value, which is thresholded as

$$X_r = \begin{cases} 1 & \text{if } W_r - thresh \geq 0 \\ 0 & \text{if } W_r - thresh < 0 \end{cases} \tag{17}$$

where X_r is the new value assigned to the center pixel, *thresh* is the threshold. For the textures used a threshold of 0.9 was found to be most appropriate by experimentation. An energy value is calculated for textures with different sets of filters. The filters that maximize the energy value given below are used,

$$T\_e = \frac{1}{N_1 N_2}\sum_{i=1}^{N_1}\sum_{j=1}^{N_2} X(i,j) \tag{18}$$

where T_e is the energy value of the new thresholded matrix X(i,j), N_1 and N_2 are the size of the matrix. The domain of the normalized energy values obtained from Eqn. (18) range from 0 to 1. The filters have been decimated to be of square size to speedup computations.

3.1.2 Feature extraction

A set of features are computed from the response of the image samples to the Gabor filters. They are unichannel features given by

$$E_{dab} = \sqrt{\left(\sum_{u,v} G_{dab}^{2}(x,y)\right)} \tag{19}$$

where E is the energy in the filtered image, d is a color channel and a is the scale of the filter. The interchannel features between different color channels d and d' with a and a' denoting the scales of the filters is computed as

$$I_{dd'aa'b}^{2} = 2 - \underbrace{2\sum_{u,v} \frac{G_{dab}(x,y)G_{d'a'b}(x,y)}{E_{dab}E_{d'a'b}}}_{R_{dd'aa'b}} \tag{20}$$

where $R_{dd'aa'b}$ is the zero offset normalized cross-correlation between $G_{dab}(x,y)$ and $G_{d'a'b}(x,y)$. These features have been proposed and used in [14]. Gabor filters of different orientations and scales are convolved with image samples and Eqs. (19-20) are computed which constitute the feature set.

3.2 Feature extraction using wavelet methods

The wavelets can be broadly classified into: continuous and discrete wavelets. The discrete wavelets are further classified as : non-orthogonal, biorthogonal or orthogonal wavelets. Non-orthogonal wavelets are linearly dependent and redundant frames. Orthogonal wavelets are linearly independent and complete in $L^2(R)$. A family of real orthonormal bases $y_{m,n}(u)$ obtained through translation and dilation of a kernel function $y(u)$ known as the mother wavelet is used to decompose the signal or image.

$$y_{m,n}(u) = 2^{-m/2} y(2^{-m}u - n) \tag{21}$$

where m and n are integers. Due to the orthonormal property, the wavelet coefficients of a signal f(u) can be easily computed via

$$c_{m,n} = \int_{-\infty}^{+\infty} f(u) y_{m,n}(u) du \tag{22}$$

To construct the wavelet $y(u)$, the scaling function $\phi(u)$ is first determined which satisfies the two-scale difference equation [23]

$$f(u) = \sqrt{2} \sum_k h(k) f(2u - k) \tag{23}$$

Then, the wavelet kernel $y(u)$ is related to the scaling function via

$$y(u) = \sqrt{2} \sum_k g(k) f(2u - k) \tag{24}$$

where

$$g(k) = (-1)^k h(1 - k) \tag{25}$$

g and h are the wavelet and scaling filters.

An M-level wavelet decomposition of a signal f(u) is:

$$f(u) = \sum_{n \in Z} s_{(M)}(n) f_{M,n} + \sum_{m=1}^{M} \sum_{n \in Z} d_{(m)}(n) y_{m,n} \tag{26}$$

where $s_{(M)}$'s are the expansion coefficients and $d_{(m)}$'s are the wavelet coefficients. This can be extended to the 2-D case using separable 2-D scaling and wavelet functions as tensor products of the 1-D compliments [4]:

$$\begin{aligned} h_{LL}(k,l) &= h(k).h(l) \quad & h_{LH}(k,l) &= h(k).g(l) \\ h_{HL}(k,l) &= g(k).h(l) \quad & h_{HH}(k,l) &= g(k).g(l) \end{aligned} \tag{27}$$

The 2-D decomposition of a textured image can be done iteratively using the above equations applying them to the approximate subimage at each decomposition level M, which yields a pyramid structure as shown in Fig. 2. This is the PWT, which results in 4 subimages at each level of decomposition. The energy features are computed for each of the subimages:

$$e = \frac{1}{N_1 N_2} \sum_{i=1}^{N1} \sum_{j=1}^{N2} | C_{ij} | \tag{28}$$

Where C_{ij} are the coefficient values of the subimages, N_1 and N_2 are the size of the subimages such that $1 \le i \le N_1, 1 \le j \le N_2$. The standard deviation and residual energy features have also been used with the PWT method as they increase the discriminating capability. They are given by

$$Std.dev = \left[\frac{1}{N_1 N_2} \sum_{i=1}^{N_1} \sum_{j=1}^{N_2} \left(C_{ij} - MN \right)^2 \right]^{1/2} \tag{29}$$

$$residual\_e = \frac{1}{N_1 N_2} \sum_{i=1}^{N_1} \sum_{j=1}^{N_2} \left| C_{ij} - MN \right| \tag{30}$$

where MN is the mean value. Eqs. (28-30) are computed for each subimage and constitute the feature vector.

If the wavelet transform is computed for the approximate and detail images at each level, then a complete tree structure is obtained called the wavelet packet transform. This is not used here as it yields very high order feature space. The TWT is instead applied, where a subimage is further decomposed only if its energy e is greater than or equal to a multiple of the highest subimage energy value in that level.

$$e \ge K e_{\max} \tag{31}$$

where K is a constant less than 1 used to select subimages. A K value of 0.15 is used. The energy values that satisfy this criterion form the feature vector.

3.3 Feature Selection and Classification

As supervised classification using a distance classifier has been used, a simple measure of separability has been adopted for feature selection, to be consistent with the classification algorithm. For all feature extraction methods, a feature selection procedure [24] that uses the distance between the means of each feature is used to quantify the separation between classes. A training matrix is constructed from a fixed number of training samples for each class, whose rows are feature values and columns are samples or observations. The matrix Y_{ij} is computed which contains the means for each feature *i* in class *j*. A mean value for each feature *i* is computed from all samples which forms the vector M. The sum of the distances of each feature from M is computed as

$$D_i = \sum_{j=1}^{J} \left| Y_{ij} - M_i \right| \tag{32}$$

where Y is the mean training matrix, *i* is the feature index such that $i \leq$ L the number of features, *j* is the class index and J is the total number of classes. D_i is sorted in ascending order. Features are selected from the first index and the number of features selected depends on the number of classes in the classification problem.

The selected features constitute the new training matrix. The classifier is then used to recognize unknown samples from the color images. A distance classifier is used due to its simplicity and speed. The effectiveness of distance measures depends on accurate estimation of mean and covariance. The Mahalanobis distance classifier is used in the experiments and is given by:

$$D_J(F) = \left\{ (F - A_J)^T \, \Sigma_J^{-1} (F - A_J) \right\} \tag{33}$$

where F is the feature vector calculated from an unknown sample to be classified in one of the J classes. A is the sample mean and Σ is the covariance matrix computed from the training matrix of each class J. The advantage of the Mahalanobis distance measure is that it is faster and has a degree of direction sensitivity via the covariance matrix $\sum$.

4. EXPERIMENTAL RESULTS

4.1 Experiments with test textures

Different color texture images are used for the experiments described in this Section [25,26]. The original images are RGB color images of size 512 x 512. Figs. 3, 4 and 5 show samples of the texture images used in the experiments. A total of 256 distinct samples are extracted by sequential sampling with a non overlapping window of size 32 x 32 from each color image. Out of these, features computed from 64 samples are used for training the classifier and the remaining 192 samples are used for testing. The general experimental setup for the methods is described below.

- *Training Phase*

1) In the case of Gabor method, the training texture sample is convolved with the Gabor filters. In the case of wavelet method, the sample is decomposed into subimages using wavelet filters as per the PWT or TWT method.
2) Features are computed from each filtered image in the case of the Gabor method and from each subimage in the case of the wavelet methods. A training feature vector is created for each training sample.
3) Steps 1-2 are repeated for each training sample.
4) Feature selection algorithm is applied to the training feature matrix.

- *Classification Phase*

5) Step 1 is executed for an unknown testing sample.
6) The selected features obtained from the feature selection algorithm are computed for this sample.
7) The classifier recognizes the unknown sample in one of the classes.
8) Steps 5-7 are repeated for each testing sample.

4.1.1 Gabor filtering method

The experiments are conducted with each color space. First experiment constitutes 6 class experiments using the textures in Fig. 3. Three sets of experiments by randomly selecting 6 textures from the database is conducted. The respective color space transformation is applied. Filters selected using the procedure of Section 3.1.1 for the texture databases considered here have frequencies $\in \{0.25, 0.5\}$, $\sigma \in \{0.05, 0.1, 0.2, 0.25\}$ and orientation $\in \{0°, 45°, 90°\}$. The filters are of size 8x8 and 16x16. Features are computed and selected as described in Sections 3.1.2 and 3.3. The results using various color spaces are tabulated in Table 1. On comparison with results using just gray scale values, using color cues

gives higher correct classification rates. Good results are obtained with all color spaces, the *rgb* chromaticity space and chromaticity values from HIS space perform best. The interchannel features (Eqn. 20) are well separable using the chromaticity information of the color textures. This is also the case in the 12 class experiments. Here, different types of covering materials such as weave and leather are used (Fig. 4). The HSV and *rgb* space have performed well as shown in Table 2. For testing the Gabor algorithm further experiment was done with 32 different textures (Fig. 5). These textures constitute different types of marbles, leathers, tiles and paper. The HSV space performs best followed by the L*a*b* and *rgb* spaces. As number of classes increases, more features are required to attain class separability. This is achieved with interchannel features. The perceptually uniform spaces are the best choice followed by the *rgb* space. This shows that computing the correlation between channels at the feature level improves classification with three channels. Table 3 gives the classification accuracy for each texture. The average Percentage of Correct Classification (PCC) for the 6 class, 12 class and 32 class experiments are 96.34%, 99.74% and 95.64%, respectively. The unichannel and interchannel features provide information about the texture spatial structure, color properties and details of the spatial structure from different color channels, respectively. This makes the Gabor method perform well in all experiments.

4.1.2 Wavelet methods

First, the three six class experiments are conducted using the PWT and TWT methods with all the color representations. The Daubechies wavelet filters [23] have been used in all experiments for consistency and due to their orthonormal property and suitability for texture classification. The filters are of size 4x4. In the PWT method, the maximum number of levels of decomposition is 4. Feature computation and selection process outlined in Sections 3.2 and 3.3 are applied. The results tabulated in Table 4 show that the use of color cues results in higher classification rates than with just gray scale values. The chromaticity and luminance values from HIS space followed by the HSV space give best results. The *rgb* space has also performed well. For the 12 class and the 32 class experiment the best color space is the L*a*b* followed by the HSV space as shown in Tables 2 and 3, respectively. In the 6 class experiments the textures are well distinguishable, while in the 12 and 32 class experiments there are many self similar textures, here the residual channel

energies from each channel of the HVS and L*a*b* spaces have more separability and hence results in higher classification accuracy.

The results using the TWT for the three six class experiments are shown in Table 5. The maximum number of levels for wavelet decomposition is 4. As can be seen the classification accuracies are good but less compared to PWT. The TWT uses the criterion given in Eqn. (31), which is not satisfied for different values of K by the individual channel features for the 12 and 32 class experiments and does not have much significance with the color channels. Hence, this method does not yield good results for higher-class experiments. However, on eliminating the criterion the TWT reduces to the PWT algorithm, which has given good results. Also, introducing the criterion checking increases the computational time of the wavelet algorithm especially with multiple channels. Therefore, the PWT method is found to be more suitable for higher-class problems. It results in PCC's of 93.31%, 95.83% and 93.46% for the 6 class, 12 class and 32 class experiments, respectively. While, average PCC using TWT for the 6 class experiments is 89.72%.

The color spaces add 1 or two more channels for feature extraction resulting in an increase in feature dimensionality. To handle the problem of curse of dimensionality, an efficient feature selection process that ranks the features in order of maximum separability as outlined in Section 3.3. has been used. For the 6 class experiments the number of feature selected are 8. For the 12 and 32 class experiments they are 13 and 22, respectively.

4.2 Classification of composite color image

In this experiment, the Gabor method, PWT and TWT methods are applied to classify a composite image with 4 classes shown in Fig. 6 (a). Table 6 shows the time taken for classifying the image applying the various methods to the color spaces, on a Sun Ultra 2 workstation. For estimating the computational cost on an equal footing, all methods use a 32x32 sliding window without overlapping. All the methods produced 100% correct classification, the classified image is shown in Fig. 6 (b). The Gabor method using the chromaticity and luminance information from HIS space is the fastest followed by the *rgb* space. Gabor filter selection process is not included in the timing, as it is trivial and can be done as a one time operation for a database of textured images. The TWT method is the most computationally intensive due to the additional steps involved in checking for the energy criterion to perform further subimage decomposition. The PWT is faster than the TWT method. Fig. 6(c) shows a pixel based classification of the image using the Gabor method applied to

the chromaticity and luminance channels of the HIS color space and Fig. 6 (d) shows pixel based classification using PWT method applied to *rgb* space. For both methods a sliding window of size 32 x 32 with an overlap of 31 pixels is used. Five unichannel features have been used with the Gabor method. Three energy and two average residual features have been used with the PWT method. Both images show good performance and the Gabor method has lesser misclassified pixels at the boundary between textures.

4.3 Classification of LANDSAT image

Fig. 7(a) is an original image of an area of San Juan city in Puerto Rico taken by the Landsat TM satellite. The Landsat image has channels in the visible spectrum and InfraRed (IR) spectrum. Out of the seven channels of the Landsat image, the R, G, and B channels of the visible spectrum are chosen, as the dominant vegetation regions in the image are well represented in these Landsat sensor channels. Moreover, the idea is to estimate the accuracy of the methods with the visible color channels. The *rgb* chromaticity values of the R, G and B channels are used. The image has 4 main classes: ocean, buildings, grassland and hilly vegetation. The ground truth data is based on a topographic map of the area. The segmented image using Gabor method is shown in Fig. 7(b). A sliding window of size 16x16 with an overlap of 15 pixels is used and is assigned a class number after classification. The best filters selected are of size 8 x 8, at 45°, 90° orientation and σ values are .05, 0.1 and 0.2. The best features are found to be unichannel features from R and G channels. The classification result in Fig. 7(b) is very good with a misclassification error rate of 10.75%. The major error is the water body in the land, which is misclassified as grassland. This may be due to the sensor registration of the water body in the channel G, which is really a marshland, rather than a clear water body. TWT method using *rgb* space also gives good results with an error rate of 15.42% as shown in shown in Fig. 7 (c). There are more misclassifications here in the grassland, which are recognized as hilly vegetation. The water body is classified as hilly vegetation.

5. CONCLUSIONS

Two main approaches for texture based image classification have been evaluated with various color spaces. All experiments show that the addition of color cues improves classification over the use of gray scale values only. The Gabor filtering method is found to be a universal method that performs well with all color spaces. The filter selection

process and the unichannel and interchannel features allow the method to be adaptive to different color cues. Results using wavelet methods show that they can be used for color image classification with the addition of standard deviation and residual energy features. The PWT has performed superior to TWT method. For higher class problems, both Gabor and PWT methods perform best with the perceptually uniform spaces, HSV and L*a*b*. For example, the HSV space gives an overall PCC of 95.96%.

For smaller class problems, the chromaticity and luminance channels alone is sufficient rather than using all three channels of the color space thereby saving the additional computations involved with one extra channel. The individual channels R, G and B of the RGB space has been shown to perform poorly in previous reports [18]. However, from this work it is seen that the three channel chromaticity information *rgb* computed from RGB space produces good results comparable to the perceptually uniform spaces which is also proved from the classification results of the Landsat 7 image.

6. ACKNOWLEDGEMENTS

This work was partially supported by NSF grant EIA 9977071, NASA grant NCCW-0088, NASA grant NCC5340 and the Department of Electrical and Computer Engineering at the University of Puerto Rico at Mayagüez.

7. REFERENCES

1. G. W. Wyszecki, S. W. Stiles, *Color Science: Concepts and Methods, Quantitative Data and Formulas*. New York, Wiley (1982).
2. R. M. Pickett, *Visual analysis of texture in the detection and recognition of objects. Picture Processing and Psychopictorics*, pp. 298-308, Academic Press, New York (1970).
3. A.. K. Jain, R. P. W. Duin, J. Mao, "Statistical pattern recognition: a review," *IEEE Trans. PAMI*, 22(1), 4-35 (2000).
4. T. Randen and J. H. Husoy, "Filtering for texture classification: a comparative study," *IEEE Trans. PAMI*, 21(4), 291-310 (1999).
5. C. S. Lu, P. C. Chung, C. F. Chen, "Unsupervised texture segmentation via wavelet transform," *Pattern Recognition*, 30(5), 729-742 (1997).

6. E. Salari, Z. Ling, "Texture segmentation using hierarchical wavelet decomposition," *Pattern Recognition*, 28(12), 1819-1824 (1995).

7. M. Unser, "Texture classification and segmentation using wavelet frames," *IEEE Trans. IP*, 4(11), 1549-1560 (1995).

8. O. Pichler, A. Teuner, B. J. Hosticka, "A comparison of texture feature extraction using adaptive Gabor filtering, pyramidal and tree structured wavelet transforms," *Pattern Recognition*, 29(5), 733-742 (1996).

9. G. Paschos, K. P. Valavanis, "A Color Texture Based Visual Monitoring System For Automated Surveillance," *IEEE Trans. on Systems, Man and Cybernetics*, 29(1), 298-306 (1999).

10. C. –S. Fuh, S. –W. Cho, K. Essig, "Hierarchical color image region segmentation for content-based image retrieval system," *IEEE Trans. IP*, 9(1), 56-162 (2000).

11. T. Gevers, W. M. Smeulders, "PicToSeek: combining color and shape invariant features for image retrieval," *IEEE Trans. IP*, 9(1), 102-118 (2000).

12. A. Mojsilovic et al, "Matching and retrieval based on the vocabulary and grammar of color patterns," *IEEE Trans. IP*, 9(1), 38-53 (2000).

13. M. J. Vrhel, H. J. Trussell, "Color device calibration: A mathematical formulation," *IEEE Trans. IP*, 8(12), 1796-1806 (1999).

14. A. Jain, G. Healey, "A multiscale representation including opponent color features for texture recognition," *IEEE Trans. IP*, 7(1), 124-128 (1998).

15. J. Bennett, A. Khotanzad, "Multispectral random field models for synthesis and analysis of color images," *IEEE Trans. PAMI*, 20(3), 327-332 (1998).

16. P-H. Suen, G. Healey, "Modeling and classifying color textures using random fields in a random environment," *Pattern Recognition*, 32, 1009-1017 (1999).

17. M. Mirmehdi, M. Petrou, "Segmentation of color textures," *IEEE Trans. PAMI*, 22(2), 142-159 (2000).

18. G. Paschos, "Perceptually uniform color spaces for color texture analysis: an empirical evaluation," *IEEE Trans. IP*, 10(6), 932-037 (2001).

19. G. V. De Wouwer et al., "Wavelet correlation signatures for color texture characterization," *Pattern Recognition*, 32(3), 443-452 (1999).

20. W. K. Pratt, *Digital Image Processing*, John Wiley & Sons (1991).

21. F. Truchetet et al, "High quality still color image compression," *SPIE Optical Engineering*, 39(2), 409-414 (2000).

22. A. R. Smith, "Color Gamut Transfrom Pairs," *Proceedings of SIGGRAPH'78* (1978).

23. I. Daubechies, "The wavelet transform, time-frequency localization and signal analysis," *IEEE Trans. Information Theory*, 32(5), 961-1005 (1990).

24. R. O. Duda, P. E. Hart, *Pattern Classification and Scene Analysis*, Wiley-Interscience, NY (1973).

25. VisTex, *Color image database*, http://www-white.media.mit.edu/vismod/imagery/Vision Texture. MIT Media Lab (1995).

26. PIXAR. *A collection of photographic textures*, Vol. 2 (2000).

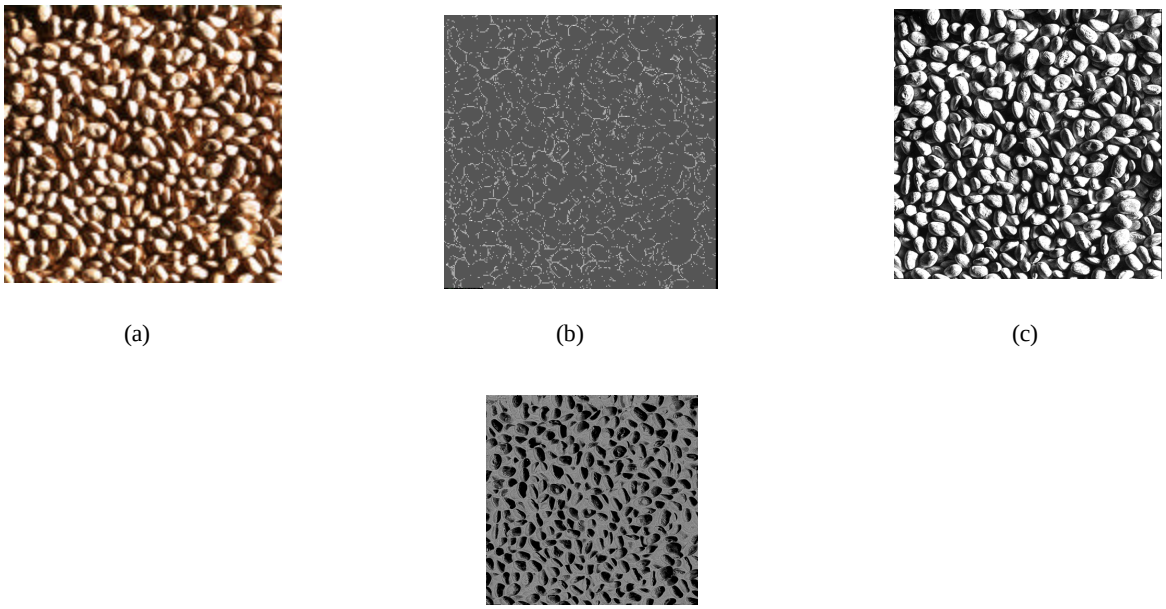

(a) (b) (c)

(d)

Fig. 1. Chromaticity and luminance images (a) Original RGB image, (b) xy image, (c) Y image, (d) H_2 image

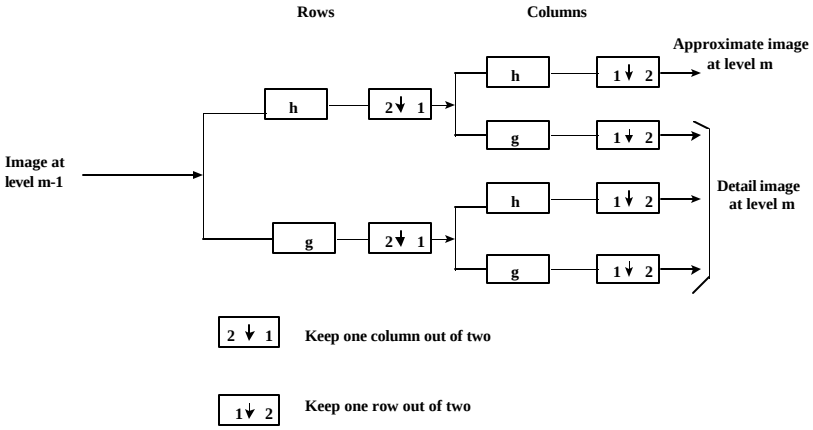

Fig. 2. Wavelet decomposition of an image

Fig. 3. Samples of textures for 6 class experiments

Fig. 4. Samples of textures for 12 class experiments

Fig. 5. Samples of textures for 32 class experiments

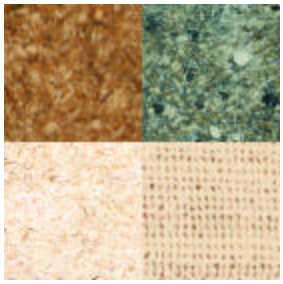

(a)

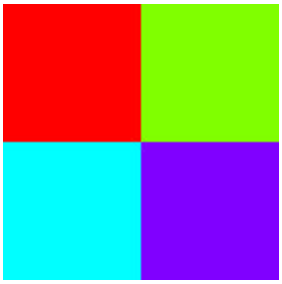

(b)

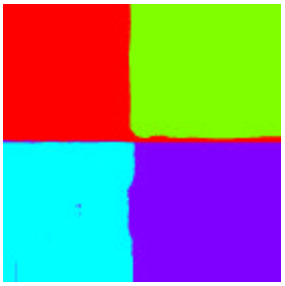

(c)

(d)

Fig. 6. (a) 4 texture composition image, (b) Classification using methods listed in Table 6, (c) Pixel based classification using Gabor method, (d) Pixel based classification using PWT method

(a)

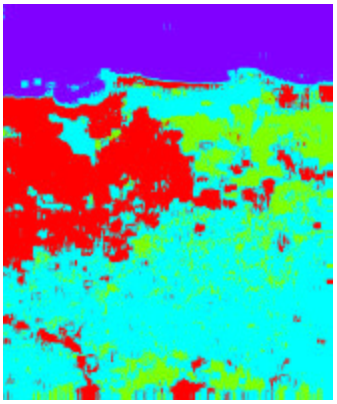

(b)

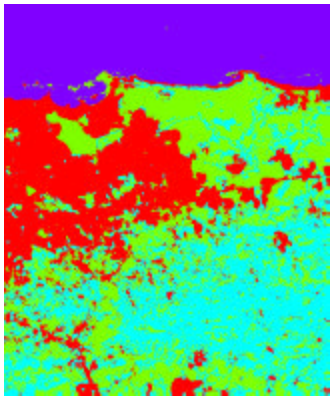

(c)

Fig. 7. (a) Original Landsat image of San Juan area, Puerto Rico, (b) Classified image using Gabor method, (c) Classified image using TWT method

Texture	chromaticity & luminance		HSV	L*a*b*	*rgb*	Gray scale
	xyY	HIS				
Flower	86.72	96.88	98.44	92.97	99.22	90.63
Brick	100	100	92.97	100	100	77.34
Water	96.10	93.36	94.14	95.32	100	95.32
Sand	100	99.61	98.44	100	100	84.38
Grass	99.61	100	93.36	97.62	100	95.71
Food	100	98.05	94.14	98.44	98.83	79.69
Leaves	100	99.22	100	100	100	100
Metal	92.19	100	96.09	96.09	92.19	96.88
Fabric	100	100	100	100	100	95.31
Misc.	96.88	96.88	95.31	96.88	99.22	92.19
Stone	89.06	84.38	96.88	77.34	100	95.31
Terrain	85.94	97.38	97.66	99.22	100	96.88
Tile	87.5	97.66	85.94	94.53	100	98.44
Wood	90.19	89.45	99.22	85.94	100	90.63
Average	**94.59**	**96.63**	**95.90**	**95.31**	**99.25**	**92.05**

Table 1. Classification accuracy (%) for Gabor method for 6-class experiments

Texture Class	Gabor method				PWT	
	chromaticity & luminance (HIS)	HSV	L*a*b*	*rgb*	HSV	L*a*b*
1	100	100	100	100	100	100
2	100	100	100	100	100	100
3	100	100	94.53	100	93.75	97.66
4	100	100	100	100	100	99.22
5	100	100	100	100	100	100
6	100	100	100	100	100	100
7	100	100	100	100	100	100
8	100	100	100	100	100	100
9	100	100	98.44	100	100	100
10	100	100	100	100	100	100
11	100	99.22	98.44	100	99.22	100
12	100	100	96.88	100	100	100
Average	**100**	**99.94**	**99.02**	**100**	**91.91**	**99.74**

Table 2. Classification accuracy for Gabor and PWT methods for the 12- class experiment

Texture Class	Gabor method				PWT	
	chromaticity & luminance (HIS)	HSV	L*a*b*	*rgb*	HSV	L*a* b*
1	100	100	100	100	99.22	100
2	100	92.19	100	100	100	100
3	100	100	100	100	99.22	100
4	100	100	100	100	99.22	100
5	100	99.22	100	96.09	99.22	98.44
6	100	100	100	100	100	100
7	92.19	94.53	95.31	99.22	90.63	95.31
8	100	100	100	100	100	99.22
9	97.66	100	96.88	99.22	94.53	85.94
10	85.94	97.66	89.84	92.97	85.94	79.69
11	94.53	94.53	89.06	99.22	92.19	88.28
12	93.75	84.38	93.75	89.84	78.13	84.38
13	97.66	96.88	97.66	100	100	100
14	99.22	100	99.22	100	99.22	100
15	91.41	84.34	86.72	87.5	92.97	82.81
16	98.44	100	98.44	100	99.22	69.53
17	100	97.66	98.44	99.22	98.44	98.44
18	87.5	97.66	91.41	98.44	99.22	97.66
19	93.75	100	98.44	100	96.88	97.66
20	89.84	100	92.19	100	100	89.84
21	87.5	99.22	100	99.22	93.75	98.44
22	92.97	98.44	100	100	100	100
23	94.53	100	96.88	100	100	98.44
24	94.53	98.44	98.44	97.66	84.34	79.69
25	60.16	86.72	95.31	100	98.44	96.09
26	92.66	100	97.66	99.22	100	99.22
27	97.66	100	99.22	97.66	97.66	99.22
28	98.44	97.66	99.22	100	96.88	99.22
29	94.53	98.44	96.88	93.75	96.88	99.22
30	98.44	100	100	100	97.66	100
31	89.84	100	97.66	97.66	89.84	97.66
32	72.66	88.28	84.38	89.84	85.16	78.91
Average	**93.62**	**97.07**	**96.66**	**95.21**	**92.75**	**94.17**

Table 3. Classification accuracy (%) for the Gabor and PWT methods for the 32-class experiment

Texture	Chromaticity & luminance		HSV	L*a*b*	*rgb*	Gray scale
	xyY	HIS				
Flower	72.81	100	100	94.06	100	95.31
Brick	50.99	100	99.22	82.03	86.72	97.66
Water	90.24	97.15	93.75	93.75	94.53	80.86
Sand	100	99.61	96.1	80.08	99.61	93.75
Grass	96.10	100	96.88	82.42	98.05	94.14
Food	100	98.83	99.22	100	99.61	83.21
Leaves	100	100	100	100	100	89.06
Metal	97.66	100	100	99.22	100	98.44
Fabric	100	100	99.22	100	100	99.22
Misc.	92.77	99.22	96.09	83.59	91.41	55.47
Stone	97.66	98.44	85.16	62.5	93.75	76.56
Terrain	85.94	96.21	96.09	75.78	100	63.28
Tile	87.5	93.75	97.66	77.34	88.28	96.09
Wood	100	88.28	92.97	96.88	70.56	85.94
Average	**90.83**	**97.96**	**95.60**	**87.68**	**94.47**	**86.36**

Table 4. Classification accuracy (%) for the PWT method for the 6-class experiments

Texture	Chromaticity & luminance		HSV	L*a*b*	*rgb*	Gray scale
	xyY	HIS				
Flower	71.88	67.97	96.09	92.97	99.22	88.28
Brick	78.56	90.63	98.44	98.44	95.31	91.41
Water	86.96	82.42	92.97	96.88	94.54	44.54
Sand	99.61	87.5	100	100	100	98.05
Grass	99.22	75.78	97.27	98.05	96.49	77.35
Food	90.23	83.60	99.22	99.22	94.15	51.17
Leaves	100	99.22	100	100	100	55.47
Metal	96.09	100	100	99.22	99.22	73.44
Fabric	100	100	100	100	100	85.94
Misc.	88.22	99.22	94.53	98.44	88.28	78.91
Stone	100	68.75	78.13	80.47	87.5	80.47
Terrain	96.88	44.53	89.06	96.09	98.44	96.88
Tile	78.12	47.66	92.97	80.47	79.69	71.09
Wood	96.09	81.25	92.97	82.03	61.78	31.25
Average	**85.95**	**80.63**	**95.12**	**94.45**	**92.47**	**73.16**

Table 5. Classification accuracy (%) for the TWT method for the 6-class experiments

Method	Color space	Time (in seconds)
Gabor method	chromaticity & luminance (HIS)	139.5900
Gabor method	*rgb*	232.0100
PWT	*rgb*	301.9300
TWT	*rgb*	485.3500

Table 6. Timing results for classifying the image in Fig. 6 (a) to Fig. 6 (b)

FIGURE CAPTION LIST

Fig. 1. Chromaticity and luminance images (a) Original RGB image, (b) xy image, (c) Y image, (d) H_2 image

Fig. 2. Wavelet decomposition of an image

Fig. 3. Samples of textures for 6 class experiments

Fig. 4. Samples of textures for 12 class experiments

Fig. 5. Samples of textures for 32 class experiments

Fig. 6. (a) 4 texture composition image, (b) Classification using methods listed in Table 6, (c) Pixel based classification using Gabor method, (d) Pixel based classification using PWT method

Fig. 7. (a) Original Landsat image of San Juan area, Puerto Rico, (b) Classified image using Gabor method (c) Classified image using TWT method